Journal of Colloid and Interface Science 395 (2013) 277–286

Contents lists available at SciVerse ScienceDirect

Journal of Colloid and Interface Science

www.elsevier.com/locate/jcis

Analytical solution of two-fluid electro-osmotic flows of viscoelastic fluids

A.M. Afonso [a,*], M.A. Alves [a], F.T. Pinho [b]

[a] Departamento de Engenharia Química, Centro de Estudos de Fenómenos de Transporte, Faculdade de Engenharia da Universidade do Porto, Rua Dr. Roberto Frias s/n, 4200-465 Porto, Portugal

[b] Centro de Estudos de Fenómenos de Transporte, Faculdade de Engenharia da Universidade do Porto, Rua Dr. Roberto Frias s/n, 4200-465 Porto, Portugal

ARTICLE INFO

Article history:
Received 4 November 2012
Accepted 5 December 2012
Available online 22 December 2012

Keywords:
Electro-osmotic flows
Two-fluid pump
Viscoelastic fluids

ABSTRACT

This paper presents an analytical model that describes a two-fluid electro-osmotic flow of stratified fluids with Newtonian or viscoelastic rheological behavior. This is the principle of operation of an electro-osmotic two-fluid pump as proposed by Brask et al. [*Tech. Proc. Nanotech.*, 1, 190–193, 2003], in which an electrically non-conducting fluid is transported by the interfacial dragging viscous force of a conducting fluid that is driven by electro-osmosis. The electric potential in the conducting fluid and the analytical steady flow solution of the two-fluid electro-osmotic stratified flow in a planar microchannel are presented by assuming a planar interface between the two immiscible fluids with Newtonian or viscoelastic rheological behavior. The effects of fluid rheology, shear viscosity ratio, holdup and interfacial zeta potential are analyzed to show the viability of this technique, where an enhancement of the flow rate is observed as the shear-thinning effects are increased.

1. Introduction

Electro-osmotic flows (EOFs) in microfluidic devices have been studied extensively over the past decade [1–5], because they enable precise liquid manipulation and are easily miniaturized to nanosized systems. The major applications of electro-osmotic (EO) pumps are in micro flow injection analysis, microfluidic liquid chromatography systems, microreactors, microenergy systems, and microelectronic cooling systems. Fluid pumps are important elements in such microchannel networks, and promising candidates for miniaturization are electro-hydrodynamic pumps using ion-dragging effects via the so-called electro-osmosis [6] due to the inherent simplicity in producing small-sized pumps with these techniques. A comprehensive review on electrokinetic pumps has been recently published by Wang et al. [5].

Some of the above mentioned studies focused on the transport of single-phase fluids with high electrical conductivity, for which a classical EO pump is needed. An overview of fabrication methods and working principles for such systems was presented by Zeng et al. [7]. For nonpolar fluids, such as oil, traditional EOF pumping cannot be used, due to the low fluid conductivity [2].To overcome this limitation, Brask et al. [1] proposed an alternative construction that allows the use of EOF as a driving mechanism, using an electrolyte fluid with high conductivity to drag the low conductivity nonpolar fluid. Their study [1] analyzed the performance of the pump by equivalent circuit theory and computational fluid dynamic simulations.

The theoretical study of electro-osmotic flows of non-Newtonian fluids is recent and has been mainly focused in simple inelastic fluid models, such as the power-law, due to the inherent analytical difficulties introduced by more complex constitutive equations. Examples are the recent works of Das and Chakraborty [8] and Chakraborty [9], who presented explicit relationships for velocity, temperature, and concentration distributions in electro-osmotic microchannel flows of non-Newtonian bio-fluids described by the power-law model. Other purely viscous models were analytically investigated by Berli and Olivares [10], who considered the existence of a small wall layer depleted of additives and behaving as a Newtonian fluid (the skimming layer), under the combined action of pressure and electrical fields, thus restricting the non-Newtonian behavior to the electrically neutral region outside the electrical double layer (EDL). More recently, these studies were extended to viscoelastic fluids by Afonso et al. [11], who presented analytical solutions for channel and pipe flows of viscoelastic fluids under the mixed influence of electrokinetic and pressure forces, using two constitutive models: the Phan-Thien and Tanner (PTT) model [12], with linear kernel for the stress coefficient function and zero second normal stress difference [13], and the Finitely Extensible Non-linear Elastic dumbbell model with a Peterlin approximation for the average spring force (FENE-P model, cf. Bird et al. [14]). An earlier investigation with the PTT model by Park and Lee [15] was concerned with EOF in a square duct for which a numerical method was used. The analysis of Afonso et al. [11] was restricted to cases with small electric double layers, where the distance between the walls of a microfluidic device is at least

* Corresponding author.
E-mail addresses: aafonso@fe.up.pt (A.M. Afonso), mmalves@fe.up.pt (M.A. Alves), fpinho@fe.up.pt (F.T. Pinho).

0021-9797/$ - see front matter © 2012 Elsevier Inc. All rights reserved.
http://dx.doi.org/10.1016/j.jcis.2012.12.013

one order of magnitude larger than the EDL, and the fluid is well mixed and uniformly distributed across the channel. This well-mixed approximation was also considered by Park and Lee [15]. When the viscoelastic flow is induced by a combination of both electric and pressure potentials, in addition to the single contributions from these two mechanisms, there is an extra term in the velocity profile that simultaneously combines both forcings, which is absent for the Newtonian fluids where the superposition principle applies. This extra term can contribute significantly to the total flow rate, depending on the value of the relative microchannel ratio and appears only when the rheological constitutive equation is non-linear. Afonso et al. [16] extended this study to the flow of viscoelastic fluids under asymmetric zeta potential forcing, Sousa et al. [17] considered the formation of a skimming layer without polymer near the walls, and Dhinakaran et al. [18] analyzed the full PTT model with non-zero second normal stress differences, but only considering EOF without a pressure gradient. Recently, Afonso et al. [19] derived the full analytical solution for fully-developed electro-osmosis driven flow of polymer solutions described by the sPTT or FENE-P models with a Newtonian solvent.

The analytical solution of the steady two-fluid electro-osmotic stratified flow in a planar microchannel is presented in this work, assuming a planar interface between the two viscoelastic immiscible liquids. The working principle of the two-fluid pump is described in detail in Section 2. The PTT fluid considered here obeys the simplified model [12], with a linear kernel for the stress coefficient function and a zero second normal stress difference in shear [13]. The PTT model also includes the limiting case of the Upper-Convected Maxwell (UCM) fluids.

The remaining of the paper starts with the flow problem definition, followed by the presentation of the set of governing equations and a discussion of the assumptions made to obtain the analytical solution. Using this solution, the effects of the various relevant dimensionless parameters upon the flow field characteristics and pump efficiency are discussed in detail.

2. Flow geometry and definitions

The flow under investigation is the steady, fully-developed channel flow of two incompressible and immiscible layers of viscoelastic fluids which also have significantly different conductivities, as shown schematically in Fig. 1a. This type of flow can be found in some EOF pumps [1], where the non-conducting fluid located at the upper part of the system is dragged by an electrically conducting fluid at the bottom part, as illustrated in Fig. 1b. Although the origin of the coordinate system is considered at the interface between the two fluids, their thickness is not necessarily identical.

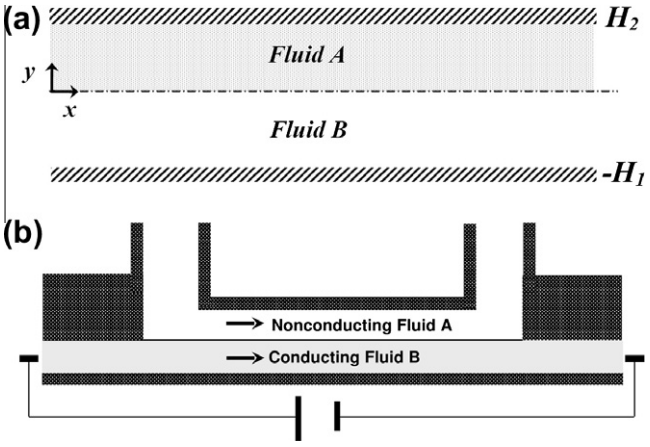

Fig. 1. (a) Illustration of the coordinate system and (b) schematic of the two-fluid EOF pump.

The migration of ions leading to the formation of the electric layers naturally arises due to the interaction between the dielectric bottom wall and the conducting fluid. Concerning the wall-fluid interface, the charged bottom wall of the channel attracts counter-ions to form a layer of charged fluid near the wall and repels the co-ions. A very thin layer of immobile counter-ions covers the bottom wall, known as the Stern layer, and is followed by a thicker more diffuse layer of mobile counter-ions. These two layers near the wall form the EDL. The global charge of the conducting fluid remains neutral, but since the EDL is thin the core of the conducting fluid is essentially neutral. Applying a DC potential difference between the two electrodes at the inlet and outlet of the bottom channel section generates an external electric field that exerts a Coulombic body force on the counter-ions of the EDL, which move along the bottom channel dragging the remaining fluid above by viscous forces.

A similar situation arises at the fluid–fluid interface, where there is also dielectric interaction leading to the formation of a second EDL in the conducting fluid next to the interface. The conducting fluid (Fluid B) moves under the forcing imposed by the Coulombic forces and drags the non-conducting fluid (Fluid A) by hydrodynamic viscous forces at the interface (cf. Fig. 1a).

The pressure difference that can be independently applied between the inlets and outlets of both the upper and the lower channels can act in the same or in the opposite direction of the electric field. Alternatively, the streamwise electric potential difference may not be imposed independently, but results from the accumulation of ions at the end of the channel due to the flow forced by an imposed pressure difference. This particular case is known as the streaming potential and implies a specific relationship between the imposed favorable pressure gradient and the ensuing adverse external electric field [20], a case which will not be analyzed in this paper for conciseness.

To analyze this system, a two-dimensional Cartesian orthonormal coordinate system (x,y) is used with the origin of the y-axis located at the fluid–fluid interface, as shown in Fig. 1a. We assume a stratified viscoelastic flow and a planar interface. The thickness of the conducting and non-conducting fluid is H_1 and H_2, respectively. The width w is assumed to be very large, such that $w \gg H_2 + H_1 = H$.

The holdup of the conducting fluid (Fluid B), R_B, is here defined as the ratio between the cross-section area occupied by the conducting fluid and the total cross-section area of the channel,

$$R_B = \frac{H_1}{H_2 + H_1} = \frac{H_1}{H}. \tag{1}$$

Similarly, the holdup of non-conducting fluid (Fluid A) is defined as

$$R_A = 1 - R_B = \frac{H_2}{H_2 + H_1} = \frac{H_2}{H}. \tag{2}$$

The electrical double layer that forms near the bottom channel wall in contact with the conducting fluid (Fluid B) has a zeta potential denoted by ζ_1. The second EDL in Fluid B, at the interface contact with fluid A, has an interfacial zeta potential (ζ_i) that depends on the properties of the two fluids and also varies with the pH value, the concentration of ions in the conducting fluid and the presence of ionic surfactants [2]. This interfacial zeta potential influences the potential distribution in the two EDLs, hence the electro-osmotic force distribution and consequently the flow rates.

3. Theoretical model of the two-fluid electro-osmotic viscoelastic flow

The basic field equations describing this fully-developed laminar flow of incompressible fluids are the continuity equation,

$$\nabla \cdot \mathbf{u} = 0, \tag{3}$$

and the modified Cauchy equation,

$$\rho\frac{D\mathbf{u}}{Dt} = -\nabla p + \nabla\cdot\boldsymbol{\tau} + \rho_e\mathbf{E}, \tag{4}$$

where $\mathbf{u}$ is the velocity vector, p is the pressure, and $\boldsymbol{\tau}$ is the polymeric extra-stress tensor. The $\rho_e\mathbf{E}$ term of Eq. (4) represents a Coulombic body force per unit volume, where $\mathbf{E}$ is the applied external electric field, and ρ_e is the net electric charge density in the fluid. This term is null for the nonpolar fluid A, but needs to be quantified for the polar fluid B. The main simplifying assumptions and considerations in the current analysis are as follows: (i) the two fluids are viscoelastic (the Newtonian fluid is included in the analysis as a limiting case when the relaxation time is negligible); (ii) fluid properties are assumed to be independent of local electric field, ion concentration, and temperature (this is certainly true for dilute solutions [2], but we also consider this assumption to hold for our case); (iii) the flow is steady and fully-developed with no-slip boundary conditions at the channel walls; (iv) the two fluids are immiscible, and there is stratification with a planar interface between fluids where a second EDL forms; (v) a pressure gradient can simultaneously be imposed along the channel and (vi) the standard electrokinetic theory conditions apply [21].

3.1. PTT model constitutive equations

The polymer extra-stress $\boldsymbol{\tau}$ is described by an appropriate constitutive equation, and in this work, we consider the viscoelastic model of Phan-Thien and Tanner [12,13] (PTT model), derived from network theory arguments:

$$f(\tau_{kk})\boldsymbol{\tau} + \lambda\overset{\nabla}{\boldsymbol{\tau}} = 2\eta\mathbf{D}. \tag{5}$$

Here, $\mathbf{D} = (\nabla\mathbf{u}^T + \nabla\mathbf{u})/2$ is the rate of deformation tensor, λ is the relaxation time of the fluid, η is the viscosity coefficient, and $\overset{\nabla}{\boldsymbol{\tau}}$ represents the upper-convected derivative of $\boldsymbol{\tau}$, defined as

$$\overset{\nabla}{\boldsymbol{\tau}} = \frac{D\boldsymbol{\tau}}{Dt} - \nabla\mathbf{u}^T.\boldsymbol{\tau} - \boldsymbol{\tau}.\nabla\mathbf{u}. \tag{6}$$

The stress coefficient function, $f(\boldsymbol{\tau}_{kk})$, is given by the linear form [12]

$$f(\tau_{kk}) = 1 + \frac{\varepsilon\lambda}{\eta}\tau_{kk}, \tag{7}$$

where τ_{kk} represents the trace of the extra-stress tensor. The extensibility parameter, ε , bounds the steady-state elongational viscosity, which is inversely proportional to ε, for small ε. For $\varepsilon = 0$, the UCM model is recovered which has an unbounded elongational viscosity above a critical strain rate $\dot{\varepsilon} = 1/(2\lambda)$ [14]. For fully-developed flow conditions, for which $\mathbf{u} = \{u(y), 0, 0\}$, the extra-stress field for the PTT model can be obtained from equations (5)–(7), leading to

$$f(\tau_{kk})\tau_{xx} = 2\lambda\dot{\gamma}\tau_{xy} \tag{8}$$

and

$$f(\tau_{kk})\tau_{xy} = \eta\dot{\gamma} \tag{9}$$

where $\tau_{kk} = \tau_{xx}$, since $\tau_{yy} = \tau_{zz} = 0$ [22,23], and $\dot{\gamma}$ is the transverse velocity gradient ($\dot{\gamma} \equiv du/dy$). Then, upon division of Eq. (8) by Eq. (9), the specific function $f(\tau_{kk})$ cancels out, and a relation between the normal and shear stresses is obtained,

$$\tau_{xx} = 2\frac{\lambda}{\eta}\tau_{xy}^2. \tag{10}$$

3.2. Electric double layers in the conducting fluid (Fluid B)

The potential field within the conducting fluid B can be expressed by means of a Poisson equation:

$$\nabla^2\psi = -\frac{\rho_e}{\epsilon}, \tag{11}$$

where ψ denotes the induced electric potential, and ϵ is the dielectric constant of the fluid. In equilibrium conditions near a charged wall, the net electric charge density, ρ_e, can be described as

$$\rho_e = -2n_o ez\sinh\left(\frac{ez}{k_BT}\psi\right), \tag{12}$$

where n_o is the ion density, e is the elementary electric charge, z is the valence of the ions, k_B is the Boltzmann constant, and T is the absolute temperature. In order to obtain the velocity field for fluid B, we first need to determine the net charge density distribution (ρ_e). The charge density field can be calculated by combining Eqs. (11) and (12) under fully-developed flow conditions, to obtain the well-known Poisson–Boltzmann equation

$$\frac{d^2\psi}{dy^2} = \frac{2n_oez}{\epsilon}\sinh\left(\frac{ez}{k_BT}\psi\right). \tag{13}$$

The electro-osmotic flow is primarily caused by the action of an externally applied electric field on the charged species that exist near the bottom channel wall and in the vicinity of the interfacial surface. The distribution of the charged species in the domain is governed by the potentials at the wall and at the interface and then by the externally applied electric field. When the Debye thicknesses are small, and the charges at the wall and at the interface are not large, the distribution of the charged species is governed mainly by the ζ_1 potential at the wall and by ζ_i at the interface, and negligibly affected by the applied external DC electric field (standard electrokinetic theory). Thus, the charge distribution across fluid B can be determined independently of the externally applied electric field. Indeed, the effect of fluid motion on the charge redistribution can be neglected when the fluid velocity is small, that is, when the inertial terms in the momentum equation are not dominant (indeed they vanish under fully-developed conditions) or when the Debye thickness is small. Additionally, for small values of ψ, the Debye–Hückel linearization principle ($\sinh x \approx x$) can also be used, which means physically that the electric potential energy is small compared with the thermal energy of ions, and the Poisson–Boltzmann equation can be simplified to:

$$\frac{d^2\psi}{dy^2} = \kappa^2\psi, \tag{14}$$

where $\kappa^2 = \frac{2n_oe^2z^2}{\epsilon k_BT}$ is the Debye–Hückel parameter, related with the thickness of the Debye layer as $\xi = \frac{1}{\kappa}$ (normally referred to as the EDL thickness). This approximation is valid when the Debye thickness is small but finite, that is, for $10 \lesssim H_1/\xi \lesssim 10^3$.

Eq. (14) can be integrated subjected to the following boundary conditions: zeta potential at the bottom wall $\psi_{\|y=-H_1} = \zeta_1$ and zeta potential at the interface $\psi_{\|y=0} = \zeta_i$. The potential field becomes

$$\psi(y) = \zeta_1(\Psi_1e^{\kappa y} - \Psi_2e^{-\kappa y}) \tag{15}$$

for $-H_1 \leqslant y \leqslant 0$. Denoting $R_\zeta = \zeta_i/\zeta_1$ as the ratio of zeta potentials, then, $\Psi_1 = \frac{R_\zeta e^{\kappa H_1}-1}{2\sinh(\kappa H_1)}$ and $\Psi_2 = \frac{R_\zeta e^{-\kappa H_1}-1}{2\sinh(\kappa H_1)}$. When $R_\zeta = 1$ a symmetric potential profile is observed within the conducting fluid, as obtained by Afonso et al. [11] for the whole channel with a single conducting fluid, whereas for vanishing zeta potential at the interface, $R_\zeta = 0$, one obtains a special case discussed by Afonso et al. [16]. Finally, the net charge density distribution, Eq. (12), coupled with the Debye–Hückel linearization principle leads to

$$\rho_e = -\epsilon\kappa^2\zeta_1(\Psi_1e^{\kappa y} - \Psi_2e^{-\kappa y}) = -\epsilon\kappa^2\zeta_1\Omega_1^-(y) \tag{16}$$

where the operator

$$\Omega_p^\pm(y) = (\Psi_1e^{\kappa y})^p \pm (\Psi_2e^{-\kappa y})^p \tag{17}$$

is a hyperbolic function of the transverse variable y, that depends on the ratio of zeta potentials, R_ζ, and on the thickness of the Debye layer. For the non-conducting Fluid A, there is no potential distribution, that is, the induced potential is null as well as the corresponding electric charge density, ρ_e.

3.3. Momentum equation of the two-fluid flow

3.3.1. Conducting fluid (Fluid B)

For the conducting fluid (Fluid B), the momentum Eq. (4) reduces to,

$$\frac{\mathrm{d}\tau_{xy,B}}{\mathrm{d}y} = p_{,x} - \rho_e E_x = p_{,x} + \epsilon\kappa^2\zeta_1 E_x \Omega_1^-(y) \tag{18}$$

where $E_x \equiv -\mathrm{d}\phi/\mathrm{d}x$ and $p_{,x} \equiv \mathrm{d}p/\mathrm{d}x$. The electric potential of the applied external field, ϕ, is characterized by a constant streamwise gradient. Eq. (18) is integrated to yield the following shear stress distribution

$$\tau_{xy,B} = p_{,x}y + \epsilon\kappa\zeta_1 E_x \Omega_1^+(y) + \tau_B \tag{19}$$

where τ_B is a stress integration coefficient related to the stress at the fluid–fluid interface. It is clear that in contrast to pure Poiseuille flow, the shear stress distribution is no longer linear on the transverse coordinate. Using the relationship between the normal stress and the shear stress, Eq. (10), an explicit expression for the normal stress component is also obtained,

$$\tau_{xx,B} = 2\frac{\lambda}{\eta}\left(p_{,x}y + \epsilon\kappa\zeta_1 E_x\Omega_1^+(y) + \tau_B\right)^2. \tag{20}$$

For simplicity, subscript B will be removed from the rheological parameters of Fluid B ($\eta_B = \eta$, $\varepsilon_B = \varepsilon$ and $\lambda_B = \lambda$). Combining Eqs. (9), (19) and (20) allows to obtain the expression for the velocity gradient:

$$\begin{aligned}\frac{\mathrm{d}u_B}{\mathrm{d}y} = &\left[1 + 2\varepsilon\lambda^2\left(\frac{\epsilon E_x\zeta_1}{\eta}\kappa\Omega_1^+(y) + \frac{\tau_B}{\eta} + \frac{p_{,x}}{\eta}y\right)^2\right] \\ &\times\left(\frac{\epsilon E_x\zeta_1}{\eta}\kappa\Omega_1^+(y) + \frac{\tau_B}{\eta} + \frac{p_{,x}}{\eta}y\right).\end{aligned} \tag{21}$$

Eq. (21) can be integrated subject to the no-slip boundary condition at the lower wall ($u_{B\|y=-H_1} = 0$) leading to

$$\begin{aligned}u_B = &\frac{\tau_B}{\eta}(y+H_1)\left(1 + 2\varepsilon\lambda^2\left(\frac{\tau_B}{\eta}\right)^2\right) \\ &+\left[\frac{\epsilon E_x\zeta_1}{\eta}\right]\left(1 + 6\left(\frac{\tau_B}{\eta}\right)^2\varepsilon\lambda^2\right)\Omega_{1,1}^-(y) \\ &+2\varepsilon\lambda^2\left[\frac{\epsilon E_x\zeta_1}{\eta}\right]^2\kappa\frac{\tau_B}{\eta}\left(6\Psi_1\Psi_2\kappa(y+H_1) + \frac{3}{2}\Omega_{2,1}^-(y)\right) \\ &+2\varepsilon\lambda^2\left[\frac{\epsilon E_x\zeta_1}{\eta}\right]^3\kappa^2\left(\frac{1}{3}\Omega_{3,1}^-(y) + 3\Psi_1\Psi_2\Omega_{1,1}^-(y)\right) \\ &+\frac{1}{2}\left[\frac{p_{,x}}{\eta}\right]\left(y^2 - H_1^2\right)\left(1 + 6\varepsilon\lambda^2\left(\frac{\tau_B}{\eta}\right)^2 + \varepsilon\lambda^2\left[\frac{p_{,x}}{\eta}\right]^2\left(y^2 + H_1^2\right)\right) + 2 \\ &\times\frac{\tau_B}{\eta}\varepsilon\lambda^2\left[\frac{p_{,x}}{\eta}\right]^2\left(y^3 + H_1^3\right) + 12\frac{\varepsilon\lambda^2\left[\frac{\epsilon E_x\zeta_1}{\eta}\right]\left[\frac{p_{,x}}{\eta}\right]}{\kappa}\frac{\tau_B}{\eta}\left(\Omega_{1,2}^-(y) - \Omega_{1,1}^+(y)\right) \\ &+6\frac{\varepsilon\lambda^2\left[\frac{\epsilon E_x\zeta_1}{\eta}\right]\left[\frac{p_{,x}}{\eta}\right]^2}{\kappa^2}\left(\Omega_{1,3}^-(y) + 2\Omega_{1,1}^-(y) - 2\Omega_{1,2}^+(y)\right) \\ &+6\varepsilon\lambda^2\left[\frac{\epsilon E_x\zeta_1}{\eta}\right]^2\left[\frac{p_{,x}}{\eta}\right]\left(\Psi_1\Psi_2\kappa^2\left(y^2 - H_1^2\right) + \frac{1}{2}\Omega_{2,2}^-(y) - \frac{1}{4}\Omega_{2,1}^+(y)\right)\end{aligned} \tag{22}$$

where the operator $\Omega_{p,q}^\pm(y)$, is now defined for compactness:

$$\Omega_{p,q}^\pm(y) = (\kappa y)^{(q-1)}\Omega_p^\pm(y) - (-1)^{(q+1)}(\kappa H_1)^{(q-1)}\Omega_p^\pm(-H_1). \tag{23}$$

Eq. (22) is valid for $-H_1 \leqslant y < 0$.

It is often more convenient to work with the dimensionless form of Eq. (22). Introducing the normalizations $\bar{y} = y/H_1 = y/(R_B H)$ and $\bar{\kappa} = \kappa R_B H$, the dimensionless velocity profile in the conducting fluid can be rewritten as

$$\begin{aligned}\frac{u_B}{u_{sh}} = &\overline{\tau}_B(\bar{y}+1)\left(1 + 2\overline{\tau}_B^2\frac{\varepsilon De_\kappa^2}{\bar{\kappa}^2}\right) - \left(1 + 6\overline{\tau}_B^2\frac{\varepsilon De_\kappa^2}{\bar{\kappa}^2}\right)\overline{\Omega}_{1,1}^-(\bar{y}) \\ &+2\overline{\tau}_B\frac{\varepsilon De_\kappa^2}{\bar{\kappa}}\left(6\Psi_1\Psi_2\bar{\kappa}(\bar{y}+1) + \frac{3}{2}\overline{\Omega}_{2,1}^-(\bar{y})\right) \\ &-2\varepsilon De_\kappa^2\left(\frac{1}{3}\overline{\Omega}_{3,1}^-(\bar{y}) + 3\Psi_1\Psi_2\overline{\Omega}_{1,1}^-(\bar{y})\right) \\ &+\frac{1}{2}\Gamma(\bar{y}^2-1)\left(1 + 6\overline{\tau}_B^2\frac{\varepsilon De_\kappa^2}{\bar{\kappa}^2} + \frac{\varepsilon De_\kappa^2}{\bar{\kappa}^2}\Gamma^2(\bar{y}^2+1)\right) + 2\overline{\tau}_B \\ &\times\frac{\varepsilon De_\kappa^2}{\bar{\kappa}^2}\Gamma^2(\bar{y}^3+1) - 12\overline{\tau}_B\frac{\varepsilon De_\kappa^2}{\bar{\kappa}^3}\Gamma\left(\overline{\Omega}_{1,2}^-(\bar{y}) - \overline{\Omega}_{1,1}^+(\bar{y})\right) \\ &+6\frac{\varepsilon De_\kappa^2}{\bar{\kappa}^2}\Gamma\left(\Psi_1\Psi_2\bar{\kappa}^2(\bar{y}^2-1) + \frac{1}{2}\overline{\Omega}_{2,2}^-(\bar{y}) - \frac{1}{4}\overline{\Omega}_{2,1}^+(\bar{y})\right) \\ &-6\frac{\varepsilon De_\kappa^2}{\bar{\kappa}^4}\Gamma^2\left(\overline{\Omega}_{1,3}^-(\bar{y}) + 2\overline{\Omega}_{1,1}^-(\bar{y}) - 2\overline{\Omega}_{1,2}^+(\bar{y})\right)\end{aligned} \tag{24}$$

where $\overline{\tau}_B = \frac{\tau_B}{\eta}\frac{R_B H}{u_{sh}}$ and $De_\kappa = \frac{\lambda u_{sh}}{\zeta} = \lambda\kappa u_{sh}$ is the Deborah number based on the relaxation time of the conducting fluid (Fluid B), on the EDL thickness and on the Helmholtz–Smoluchowski electro-osmotic velocity near the bottom wall, defined as $u_{sh} = -\frac{\epsilon\zeta_1 E_x}{\eta}$. The dimensionless parameter $\Gamma = -\frac{(R_B H)^2}{\epsilon\zeta_1}\frac{p_{,x}}{E_x}$ represents the ratio of pressure to electro-osmotic driving forces. Note that for simplicity, the above terms were based on the zeta potential at the bottom wall ($\psi_{\|y=-H_1} = \zeta_1$), but could have been based instead on the interfacial zeta potential using the ratio of zeta potentials: $u_{sh} = u_{shi}/R_\zeta$, $\Gamma = R_\zeta\Gamma_i$ and $De_\kappa = De_{\kappa i}/R_\zeta$.

The normalized flow rate of the pumping Fluid B can be determined from integration of the velocity profile

$$\begin{aligned}\overline{Q}_B = &\frac{\overline{u}_B}{u_{sh}} = \int_{-H_1}^0\frac{u_B}{u_{sh}H_1}\mathrm{d}y = \frac{1}{2}\overline{\tau}_B\left(1 + 2\frac{\varepsilon De_\kappa^2}{\bar{\kappa}^2}\overline{\tau}_B^2\right) - \frac{1}{3}\Gamma\left(1 + 6\overline{\tau}_B^2\frac{\varepsilon De_\kappa^2}{\bar{\kappa}^2} + \frac{6}{5}\frac{\varepsilon De_\kappa^2}{\bar{\kappa}^2}\Gamma^2\right) \\ &+\frac{3}{2}\overline{\tau}_B\frac{\varepsilon De_\kappa^2}{\bar{\kappa}^2}\Gamma^2 - \left(1 + 6\frac{\varepsilon De_\kappa^2}{\bar{\kappa}^2}\overline{\tau}_B^2\right)\left(\frac{\overline{\Omega}_{1,1}^+(0)}{\bar{\kappa}} - \overline{\Omega}_1^-(-1)\right) \\ &+2\frac{\varepsilon De_\kappa^2}{\bar{\kappa}}\overline{\tau}_B\left(3\Psi_1\Psi_2\bar{\kappa} + \frac{3}{4}\left(\frac{\overline{\Omega}_{2,1}^+(0)}{\bar{\kappa}} - 2\overline{\Omega}_2^-(-1)\right)\right) \\ &-2\varepsilon De_\kappa^2\left(\frac{\overline{\Omega}_{3,1}^+(0)}{9\bar{\kappa}} - \frac{1}{3}\overline{\Omega}_3^-(-1) + 3\Psi_1\Psi_2\left(\frac{\overline{\Omega}_{1,1}^+(0)}{\bar{\kappa}} - \overline{\Omega}_1^-(-1)\right)\right) \\ &-12\overline{\tau}_B\frac{\varepsilon De_\kappa^2}{\bar{\kappa}^4}\Gamma\left[2\overline{\Omega}_{1,2}^+(0) - 2\overline{\Omega}_{1,1}^-(0) + \bar{\kappa}^2\overline{\Omega}_1^-(-1)\right] \\ &+6\frac{\varepsilon De_\kappa^2}{\bar{\kappa}^2}\Gamma\left(\frac{1}{2\bar{\kappa}}\overline{\Omega}_{2,2}^+(0) - \frac{2}{3}\Psi_1\Psi_2\bar{\kappa}^2 + \frac{1+2\bar{\kappa}^2}{4\bar{\kappa}}\overline{\Omega}_2^-(-1) - \frac{1}{4\bar{\kappa}}\overline{\Omega}_2^-(0)\right) \\ &-6\frac{\varepsilon De_\kappa^2}{\bar{\kappa}^5}\Gamma^2\left(\bar{\kappa}\overline{\Omega}_{1,3}^-(0) - 3\bar{\kappa}\overline{\Omega}_{1,2}^+(0) + 6\overline{\Omega}_{1,1}^+(0) - 6\bar{\kappa}\overline{\Omega}_1^-(-1)\right).\end{aligned} \tag{25}$$

3.3.2. Non-conducting fluid (Fluid A)

The derivation of the analytical solution for this fluid layer follows the same steps as for the conducting fluid, with the necessary adaptations. For the non-conducting fluid (Fluid A), the momentum conservation Eq. (4) reduces to

$$\frac{\mathrm{d}\tau_{xy,A}}{\mathrm{d}y} = p_{,x}, \tag{26}$$

since, as explained, there is no external electrical field forcing, due to low conductivity of fluid A. Eq. (26) can be integrated to yield the following shear stress distribution

$$\tau_{xy,A} = p_{,x} y + \tau_A \tag{27}$$

where τ_A is the shear stress at the fluid–fluid interface, to be quantified in the next section. Using the relationship between the normal and shear stresses, Eq. (10), the following explicit expression for the normal stress component is obtained,

$$\tau_{xx,A} = 2\frac{\lambda_A}{\eta_A}\left(p_{,x} y + \tau_A\right)^2. \tag{28}$$

Combining Eqs. (9), (27) and (28) the velocity gradient distribution in Fluid A is given by

$$\frac{du_A}{dy} = \left[1 + 2\varepsilon_A \lambda_A^2 \left(\frac{p_{,x}}{\eta_A} y + \frac{\tau_A}{\eta_A}\right)^2\right]\left(\frac{p_{,x}}{\eta_A} y + \frac{\tau_A}{\eta_A}\right) \tag{29}$$

Eq. (29) can be integrated subject to the no-slip boundary condition at the upper wall ($u_{A\|y=H_2} = 0$), leading to

$$\begin{aligned} u_A = {} & \frac{\tau_A}{\eta_A}(y - H_2)\left(1 + 2\varepsilon_A \lambda_A^2 \left(\frac{\tau_A}{\eta_A}\right)^2\right) \\ & + 2\varepsilon_A \lambda_A^2 \frac{\tau_A}{\eta_A}\left[\frac{p_{,x}}{\eta_A}\right]^2 \left(y^3 - H_{\frac{3}{2}}\right) + \frac{1}{2}\left[\frac{p_{,x}}{\eta_A}\right]\left(y^2 - H_{\frac{2}{2}}\right) \\ & \times \left(1 + 6\varepsilon_A \lambda_A^2 \left(\frac{\tau_A}{\eta_A}\right)^2 + \varepsilon_A \lambda_A^2 \left[\frac{p_{,x}}{\eta_A}\right]^2 \left(y^2 + H_{\frac{2}{2}}\right)\right) \end{aligned} \tag{30}$$

valid for $0 < y \leqslant H_2$. Introducing the normalizations $\bar{y}_A = y/H_2 = y/R_A H$ and $\bar{\kappa}_A = \kappa R_A H$, the dimensionless velocity profile can be written as

$$\begin{aligned} \frac{u_A}{u_{sh}} = {} & \overline{\tau}_A(\bar{y}_A - 1)\left(1 + 2\overline{\tau}_A^2 \frac{\varepsilon_A De_{\kappa A}^2}{\overline{\kappa}_A^2}\right) + 2\overline{\tau}_A \frac{1}{\beta^2} \\ & \times \frac{\varepsilon_A De_{\kappa A}^2}{\overline{\kappa}_A^2} \Gamma_A^2 (\bar{y}_A^3 - 1) + \frac{1}{2} \\ & \times \frac{1}{\beta} \Gamma_A (\bar{y}_A^2 - 1)\left(1 + 6\overline{\tau}_A^2 \frac{\varepsilon_A De_{\kappa A}^2}{\overline{\kappa}_A^2} + \frac{1}{\beta^2} \frac{\varepsilon_A De_{\kappa A}^2}{\overline{\kappa}_A^2} \Gamma_A^2 (\bar{y}_A^2 + 1)\right) \end{aligned} \tag{31}$$

where $\overline{\tau}_A = \frac{\tau_A}{\eta_A}\frac{R_A H}{u_{sh}}$, $\beta = \eta_A/\eta_B$ is the dynamic viscosity ratio, and $De_{\kappa A} = \frac{\lambda_A u_{sh}}{\xi} = \lambda_A u_{sh} \kappa$ is the Deborah number based on the relaxation time of fluid A, and on the EDL thickness on the bottom wall and on the corresponding Helmholtz–Smoluchowski electro-osmotic velocity (so, for simplicity, we use a single set of characteristic scales for normalization related to the bottom wall of the channel). The parameter $\Gamma_A = -\frac{(R_A H)^2}{\epsilon \zeta_1}\frac{p_{,x}}{E_x}$ represents the ratio of pressure to electro-osmotic driving forces. The normalized volumetric flow rate of the pumped Fluid A in the upper part of the channel is given by

$$\begin{aligned} \overline{Q}_A = \left(\frac{\overline{u}_A}{u_{sh}}\right) = {} & \frac{\int_0^{H_2} u_A dy}{u_{sh} H_2} \\ = {} & -\frac{\overline{\tau}_A}{2}\left(1 + 2\frac{\varepsilon_A De_{\kappa A}^2}{\overline{\kappa}_A^2}\overline{\tau}_A^2\right) - \frac{3}{2}\overline{\tau}_A \frac{\varepsilon_A De_{\kappa A}^2}{\beta^2 \overline{\kappa}_A^2}\Gamma_A^2 - \frac{2}{5}\frac{\Gamma_A^3}{\beta^3}\frac{\varepsilon_A De_{\kappa A}^2}{\overline{\kappa}_A^2} \\ & - \frac{1}{3}\frac{\Gamma_A}{\beta}\left(1 + 6\overline{\tau}_A^2 \frac{\varepsilon_A De_{\kappa A}^2}{\overline{\kappa}_A^2}\right). \end{aligned} \tag{32}$$

3.3.3. Fluid A–Fluid B interface conditions

In deriving the shear stress profiles, Eqs. (19) and (27), and all the subsequent quantities such as velocity and flow rates, two integration coefficients appeared, $\overline{\tau}_A$ and $\overline{\tau}_B$, which have to be determined from the boundary conditions at the fluid–fluid interface, namely: $\tau_{xy,A\|y=0} = \tau_{xy,B\|y=0}$ and $u_{A,\|y=0} = u_{B\|y=0}$.

Using the relationships between the shear stresses at the interface, equations (19) and (27), and those for the dimensionless velocity profiles, Eqs. (24) and (31), the variables $\overline{\tau}_A$ and $\overline{\tau}_B$ can be determined:

$$\begin{cases} \overline{\tau}_A = \frac{R_A}{R_B}\frac{1}{\beta}\overline{\tau}_B - \frac{\overline{\kappa}_A}{\beta}\Omega_1^+(0) \\ \overline{\tau}_B = \sqrt[3]{-\frac{b_1}{2} + \sqrt{\frac{b_1^2}{4} + \frac{a^3}{27}}} + \sqrt[3]{-\frac{b_1}{2} - \sqrt{\frac{b_1^2}{4} + \frac{a^3}{27}}} - \frac{a_1}{3} \end{cases} \tag{33}$$

where $a = a_2 - a_1^2/3$ and $b_1 = a_3 - a_1 a_2/3 + 2a_1^3/27$. The coefficients a_1, a_2 and a_3 are given byand $a_4 = 1 + \frac{R_\varepsilon^2}{\beta^3}\frac{\overline{\kappa}^2}{\overline{\kappa}_A^2}\left(\frac{R_A}{R_B}\right)^3$, where $R_\varepsilon = \sqrt{\frac{\varepsilon_A}{\varepsilon}\frac{\lambda_A}{\lambda}}$ is a dimensionless parameter that relates the rheological properties of the two fluids.

4. Results and discussion

In the previous section, general equations were derived for steady fully-developed two-fluid electro-osmotic stratified flow of PTT viscoelastic fluids under the mixed influence of electrokinetic and pressure gradient forcings. The different influences of the driving

$$\begin{aligned} a_1 = {} & \frac{-3\overline{\Omega}_{1,1}^-(0) - \frac{3}{2}\Gamma - 3\frac{R_\varepsilon^2}{\beta^3}\overline{\kappa}_A \Omega_1^+(0) + \frac{3}{2}\frac{R_\varepsilon^2}{\beta^3}\Gamma_A}{a_4} \\ a_2 = {} & \frac{\frac{1}{2}\frac{\overline{\kappa}^2}{\varepsilon De_\kappa^2} + \overline{\kappa}\left(6\Psi_1\Psi_2\overline{\kappa} + \frac{3}{2}\overline{\Omega}_{2,1}^-(0)\right) + \Gamma^2 - 6\frac{\Gamma}{\kappa}\left(\overline{\Omega}_{1,2}^-(0) - \overline{\Omega}_{1,1}^+(0)\right) + \frac{1}{2}\frac{1}{\beta}\frac{R_A}{R_B}\frac{\overline{\kappa}^2}{\varepsilon De_\kappa^2}}{a_4} \\ & + \frac{\frac{R_A}{R_B}\frac{R_\varepsilon^2}{\beta^3}\frac{\overline{\kappa}^2}{\overline{\kappa}_A^2}\Gamma_A^2 + 3\frac{R_\varepsilon^2}{\beta^3}\frac{R_A}{R_B}\overline{\kappa}^2\left(\Omega_1^+(0)\right)^2 - 3\frac{R_\varepsilon^2}{\beta^3}\frac{\overline{\kappa}^2}{\overline{\kappa}_A}\frac{R_A}{R_B}\Gamma_A\Omega_1^+(0)}{a_4} \\ a_3 = {} & \frac{3\Gamma\left(-\Psi_1\Psi_2\overline{\kappa}^2 + \frac{1}{2}\overline{\Omega}_{2,2}^-(0) - \frac{1}{4}\overline{\Omega}_{2,1}^+(0)\right) - \frac{1}{2}\frac{\overline{\kappa}^2}{\varepsilon De_\kappa^2}\overline{\Omega}_{1,1}^-(0) - \overline{\kappa}^2\left(\frac{1}{3}\overline{\Omega}_{3,1}^-(0) + 3\Psi_1\Psi_2\overline{\Omega}_{1,1}^-(0)\right) - \frac{1}{4}\Gamma^3}{a_4} \\ & + \frac{\frac{1}{4}\frac{1}{\beta}\frac{\overline{\kappa}^2}{\varepsilon De_\kappa^2}\Gamma_A - \frac{1}{4}\frac{\overline{\kappa}^2}{\varepsilon De_\kappa^2}\Gamma + \frac{1}{4}\frac{R_\varepsilon^2}{\beta^3}\frac{\overline{\kappa}^2}{\overline{\kappa}_A^2}\Gamma_A^3 - 3\frac{\Gamma^2}{\overline{\kappa}^2}\left(\overline{\Omega}_{1,3}^-(0) + 2\overline{\Omega}_{1,1}^-(0) - 2\overline{\Omega}_{1,2}^+(0)\right) - \frac{R_\varepsilon^2}{\beta^3}\frac{\overline{\kappa}^2}{\overline{\kappa}_A}\Gamma_A^2\Omega_1^+(0)}{a_4} \\ & + \frac{\frac{3}{2}\frac{R_\varepsilon^2}{\beta^3}\overline{\kappa}^2\Gamma_A\left(\Omega_1^+(0)\right)^2 - \frac{1}{2}\frac{\overline{\kappa}_A}{\beta}\frac{\overline{\kappa}^2}{\varepsilon De_\kappa^2}\Omega_1^+(0) - \frac{R_\varepsilon^2}{\beta^3}\overline{\kappa}^2\overline{\kappa}_A\left(\Omega_1^+(0)\right)^3}{a_4} \end{aligned} \tag{34}$$

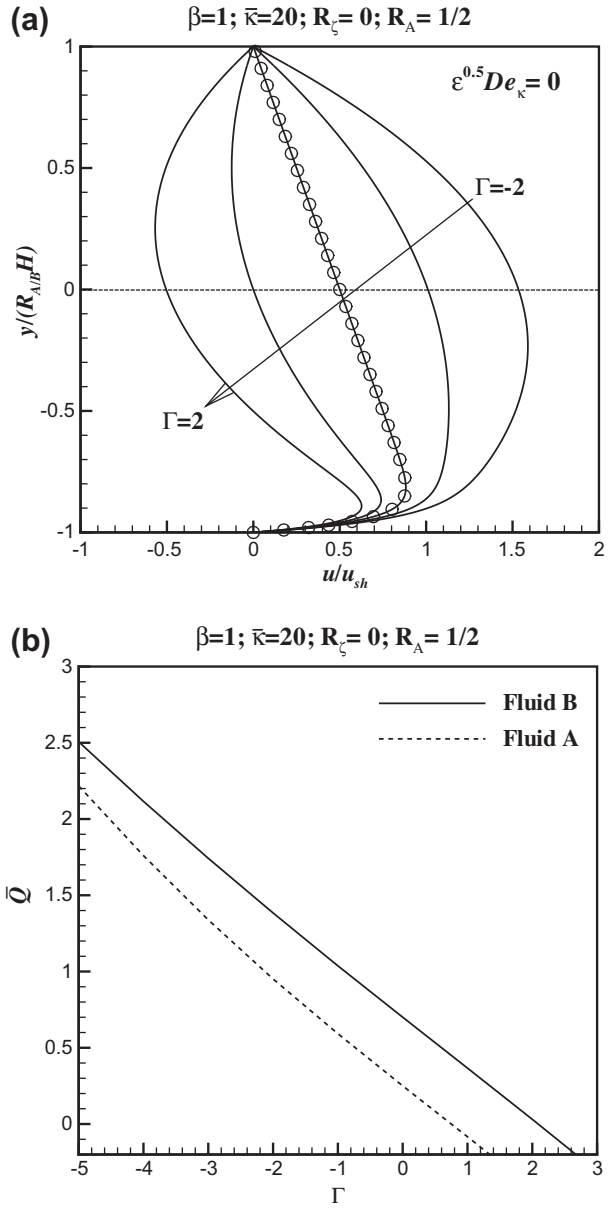

Fig. 2. Effect of the driving forces ($\Gamma = -2$, -1, 0, 1 and 2) on dimensionless (a) velocity profiles and (b) volumetric flow rate for the Newtonian–Newtonian flow configuration. Symbols represent the data from Afonso et al. [11] for ($\beta = 1$, $R_\zeta = 0$ and $\Gamma = 0$).

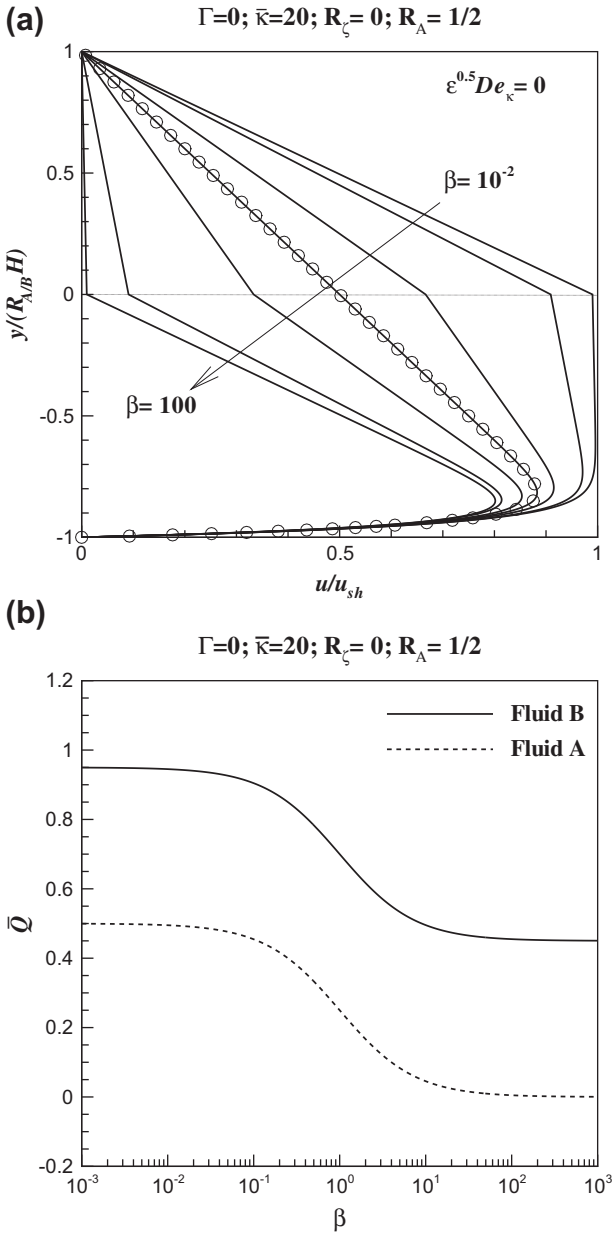

Fig. 3. Effect of the viscosity ratio ($\beta = 10^{-2}$, 10^{-1}, 0.5, 1, 2, 10 and 100) on dimensionless (a) velocity profiles and (b) volumetric flow rate for the Newtonian–Newtonian flow configuration.

forces (Γ), fluid rheology (R_ε), viscosity ratio (β), fluids holdup (R_B), and of the ratio of zeta potentials (R_ζ) on the velocity profile were explicitly incorporated in Eqs. (30), (22) and (33). In this section, we discuss in detail some limiting cases in order to understand the system fluid dynamics.

The following set of two-fluid systems is included in the general solution where the second fluid is the conducting medium: (a) Newtonian–Newtonian fluid system; (b) viscoelastic–Newtonian fluid system; (c) Newtonian–viscoelastic fluid system; and (d) viscoelastic–viscoelastic fluid system. Cases (b and d) are not discussed in this work, due to space limitations, although the derived equations also include these cases. Case (a) was studied in detail elsewhere [2], but this situation is revisited here as a starting point and for comparison with case (c), that is, in the following we analyze in detail the pumping of a Newtonian fluid by another Newtonian fluid, and, alternatively, by a viscoelastic fluid.

4.1. Newtonian–Newtonian EOF pump configuration

For the Newtonian–Newtonian fluid flow configuration, both the conducting and the non-conducting fluids are Newtonian ($De_\kappa = De_{\kappa A} = 0$). The velocity profile system equations and the dimensionless boundary condition coefficients, provided by Eq. (33), simplify to

$$\begin{cases} \frac{u_A}{u_{sh}} = \overline{\tau}_A(\overline{y}_A - 1) + \frac{1}{2\beta}\Gamma_A(\overline{y}_A^2 - 1) & \text{for} \quad 0 \leqslant \overline{y}_A \leqslant 1 \\ \frac{u_B}{u_{sh}} = \overline{\tau}_B(\overline{y} + 1) - \Omega_{1,1}^{-}(\overline{y}) + \frac{1}{2}\Gamma(\overline{y}^2 - 1) & \text{for} \quad -1 \leqslant \overline{y} \leqslant 0 \end{cases} \tag{35}$$

For small relative microchannel ratio, $\bar{\kappa} \to 1$, the double layer thickness is of the same order of magnitude as the Fluid B thickness, and the region of excess charge is distributed over the entire fluid.

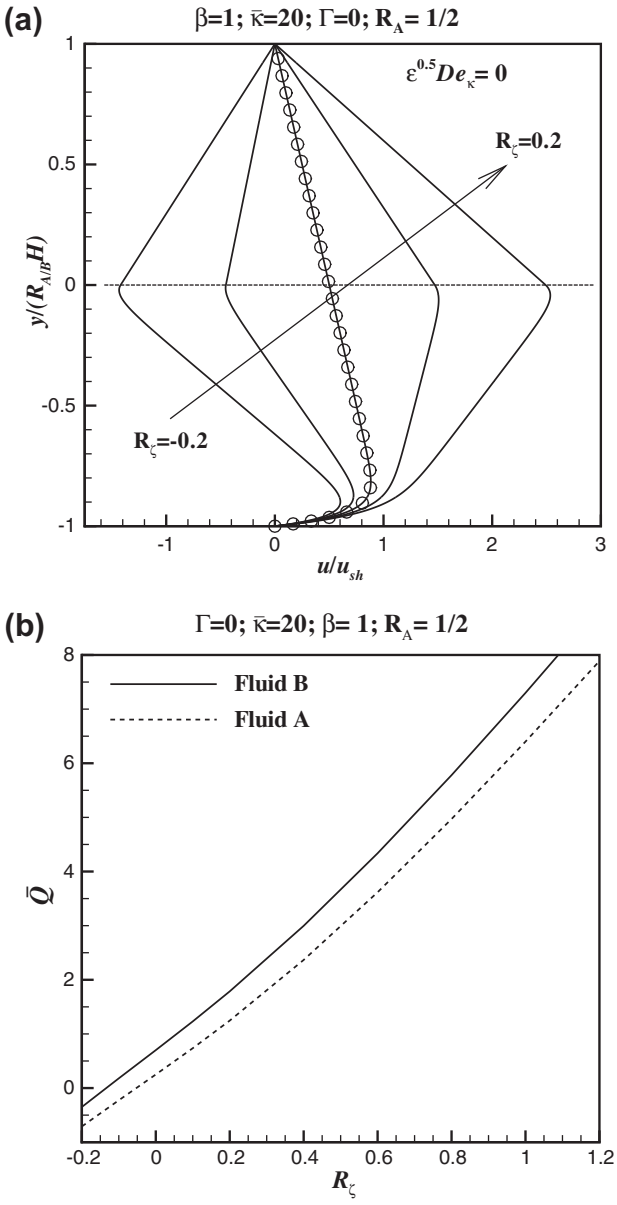

Fig. 4. Effect of the ratio of zeta potentials ($R_\zeta = -0.2$, -0.1, 0, 0.1 and 0.2) on dimensionless (a) velocity profiles and (b) volumetric flow rate for the Newtonian–Newtonian flow configuration.

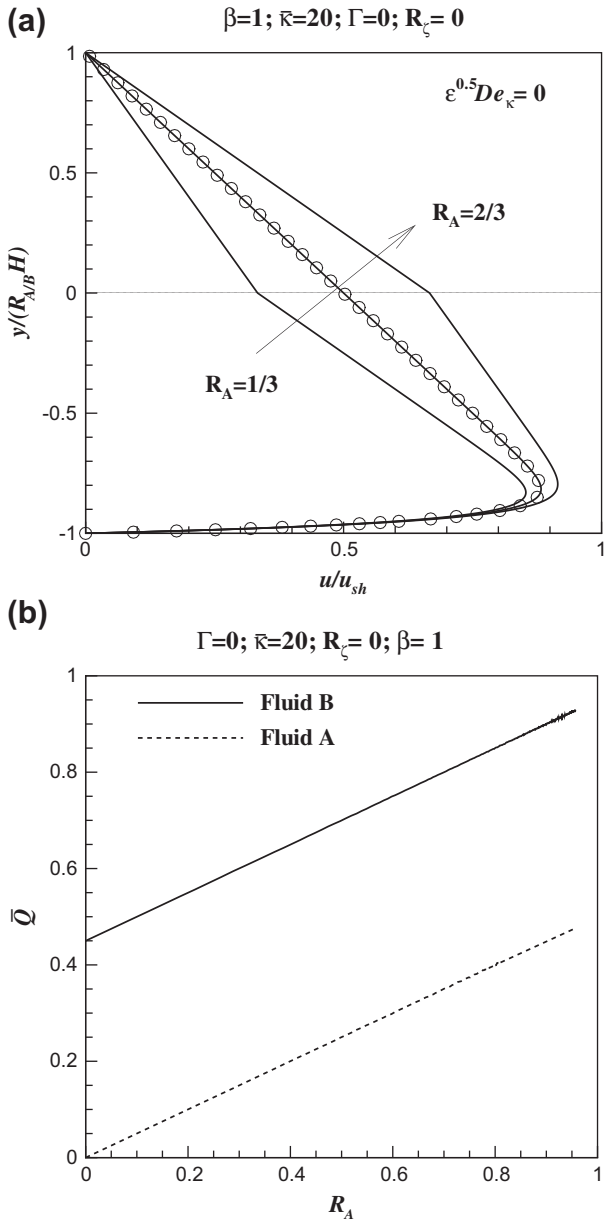

Fig. 5. Effect of the non-conducting fluid holdup on dimensionless (a) velocity profiles ($R_A = 1/3$, 1/2 and 2/3) and (b) volumetric flow rate for the Newtonian–Newtonian flow configuration.

This situation is not compatible with this solution for which the Debye–Hückel approximation was invoked, which requires $\overline{\kappa} \gtrsim 10$. In this work and as a typical example, we set $\bar{\kappa} = 20$ in all figures.

For $\Gamma = 0$, that is, when the flow is driven only by electro-osmosis, the velocity profile is a function of the wall distance, of the relative microchannel ratio, $\bar{\kappa}$, of the ratio of zeta potentials, R_ζ, and of the viscosity ratio as shown earlier by Gao et al. [2]. Also, for a single fluid situation ($\beta = 1$) and in the absence of interface zeta potential ($R_\zeta = 0$), the solution simplifies to a particular case obtained by Afonso et al. [11] (no zeta potential in the upper wall and no pressure gradient, symbols in Fig. 2a). The corresponding effect of the ratio of pressure gradient to electro-osmotic driving forces on the dimensionless flow rate is obvious (cf. Fig. 2b), increasing with favorable pressure gradients ($\Gamma < 0$) and decreasing for flows with adverse pressure gradients ($\Gamma > 0$). Obviously, the flow rate for Fluid B is higher than for Fluid A because for identical fluids height Fluid B is being forced also by electro-osmosis.

Fig. 3 shows the influence of the viscosity ratio ($\beta \equiv \eta_A/\eta_B$) on the dimensionless velocity profile (a) and volumetric flow rate (b). When the viscosity ratio decreases, the dimensionless velocity increases (cf. Fig. 3a). So, if the viscosity of the conducting fluid is much higher than the viscosity of the non-conducting fluid, an increase in the dimensionless volumetric flow rate is expected, as can be observed in Fig. 3b. However, a higher viscosity implies a lower Helmholtz–Smoluchowski electro-osmotic velocity and consequently the dimensional flow rate may actually decrease.

A major effect on the velocity profile is that due to non-zero interfacial zeta potential, as presented in the profiles of Fig. 4. When $\zeta_i/\zeta_1 > 0$, a favorable *extra* Coulombic forcing term arises in the velocity profile at the interface of the two fluids, leading to a significant increase in the volumetric flow rate. When $\zeta_i < 0$, the adverse localized electrostatic force decreases the pumping action and the corresponding dimensionless flow rate (cf. Fig. 4b).

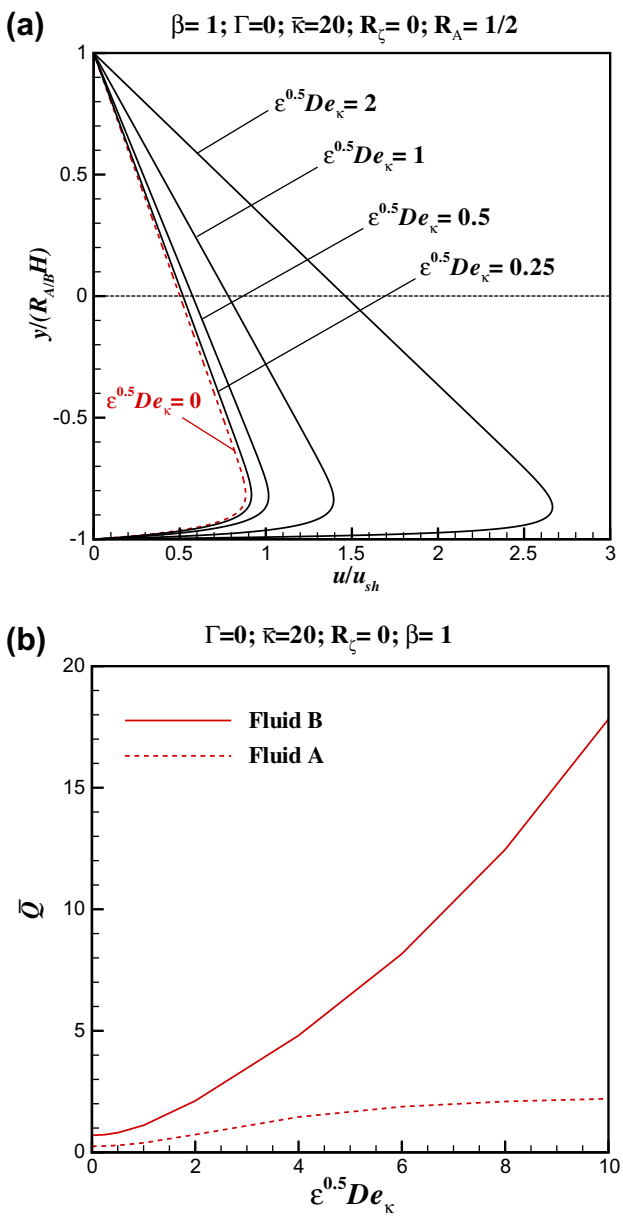

Fig. 6. Dimensionless profiles of (a) velocity and (b) volumetric flow rate as function of $\sqrt{\varepsilon}De_\kappa$.

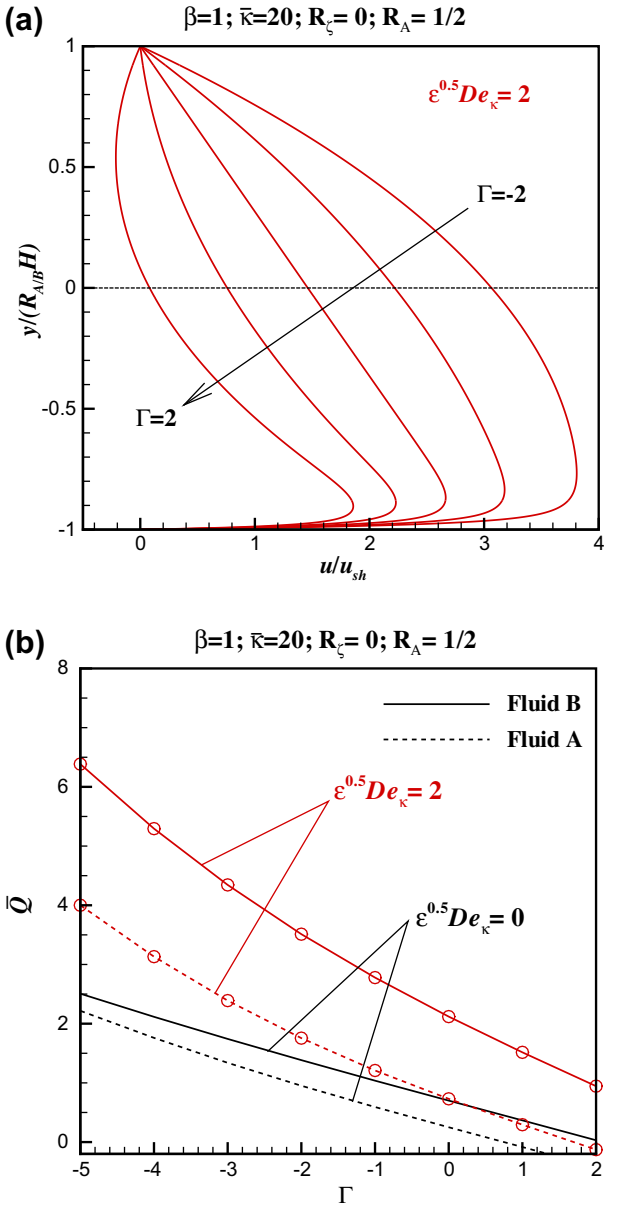

Fig. 7. Effect of the driving forces ($\Gamma = -2, -1, 0, 1$ and 2) on dimensionless (a) velocity profiles and (b) volumetric flow rate for the Newtonian–viscoelastic flow configuration.

Another important effect is due to the holdup of the non-conducting fluid. When the height of the non-conducting fluid is larger than the height of the conducting fluid ($R_A > R_B$), the normalized velocities of both fluids increase, as observed in Fig. 5a. This suggests that to obtain higher volumetric flow rates in Fluid A, the holdup of the conducting Fluid B should be kept small (cf. Fig. 5b). In fact, as the Helmholtz–Smoluchowski electro-osmotic velocity is independent of the thickness of Fluid B, as $R_A \to 1$ the fluid interface plane will tend to coincide with the regions of higher velocities. This conclusion also suggests that a better configuration for an EOF pump would be a three layer fluid flow, with the conducting fluid in contact with both the upper and lower walls, and the non-conducting fluid in the middle being dragged like a solid body, that is, a solid lubrificated by thin layers of conducting fluid in motion.

4.2. Newtonian–viscoelastic EOF pump configuration

For the Newtonian–viscoelastic fluid flow configuration, the conducting fluid is viscoelastic dragging the non-conducting Newtonian fluid. The Deborah number of the conducting fluid is non-zero ($De_\kappa \neq 0$ and $De_{\kappa A} = 0$), and the velocity profile and the non-dimensional boundary condition coefficients are given by

$$\begin{cases} \frac{u_A}{u_{sh}} = \overline{\tau}_A(\overline{y}_A - 1) + \frac{1}{2\beta}\Gamma_A(\overline{y}_A^2 - 1) & \text{for } 0 \leqslant \overline{y}_A \leqslant 1 \\ \text{Eq.(24)} & \text{for } -1 \leqslant \overline{y} \leqslant 0 \end{cases} \tag{36}$$

Fig. 6a and b presents the dimensionless velocity and volumetric flow rate profiles as a function of $\sqrt{\varepsilon}De_\kappa$, respectively. We can see that increasing the elasticity of the conducting fluid, more than doubles the velocities due to shear-thinning effects within the EDL

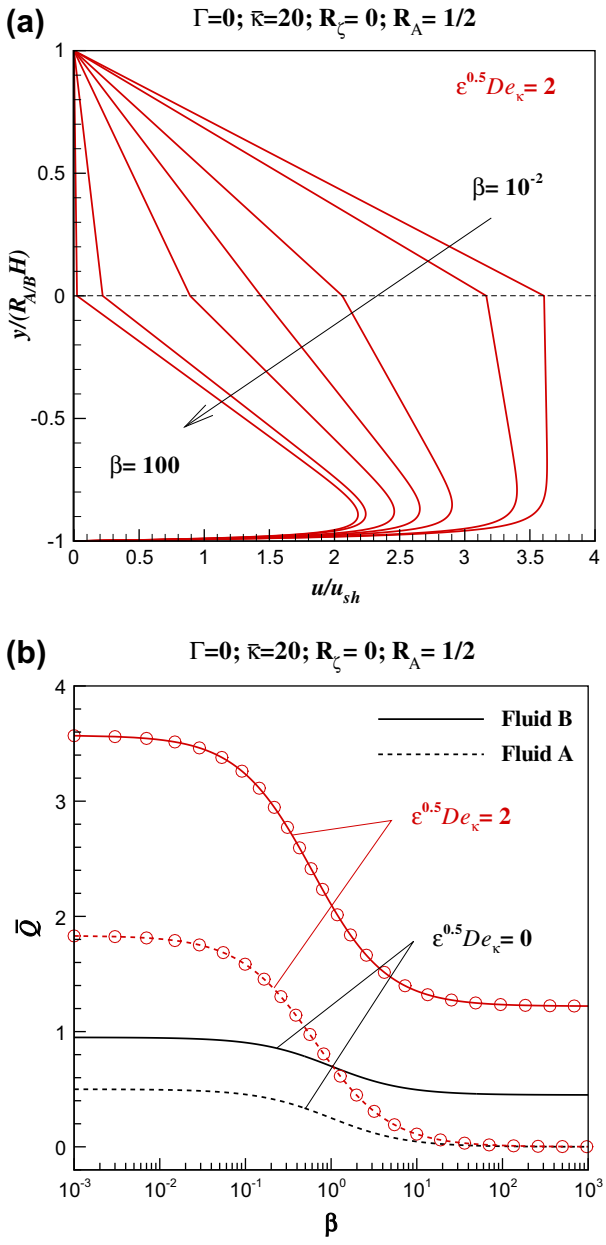

Fig. 8. Effect of the viscosity ratio ($\beta = 10^{-2}$, 10^{-1}, 0.5, 1, 2, 10 and 100) on dimensionless (a) velocity profiles and (b) volumetric flow rate for the Newtonian–viscoelastic flow configuration.

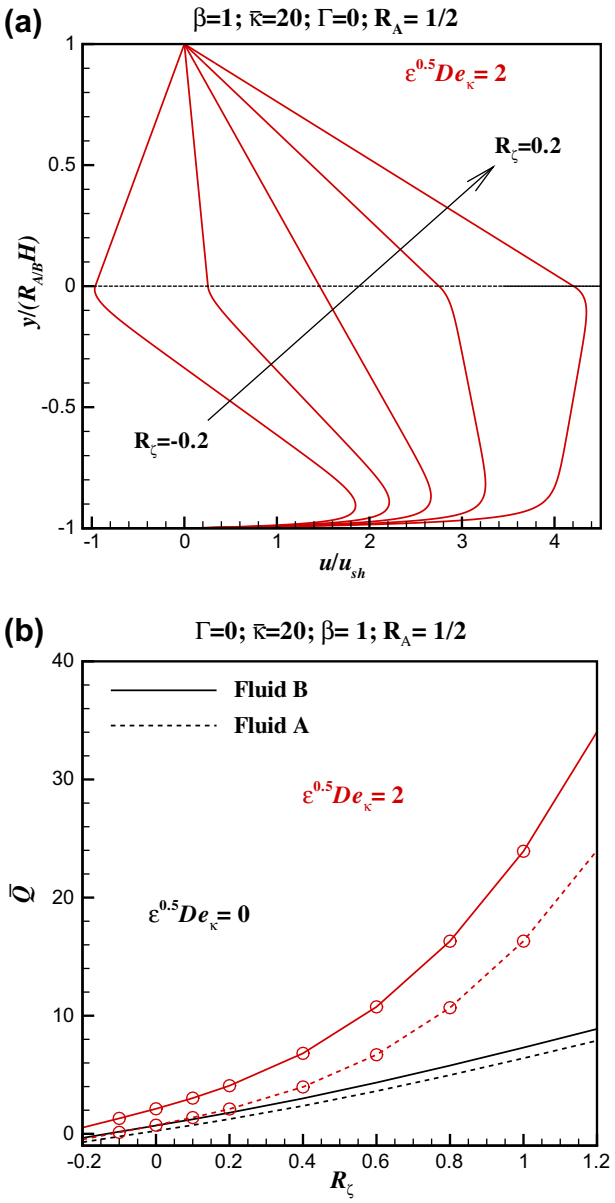

Fig. 9. Effect of the ratio of zeta potentials ($R_\zeta = -0.2$, -0.1, 0, 0.1 and 0.2) on dimensionless (a) velocity profiles and (b) volumetric flow rate for the Newtonian–viscoelastic flow configuration.

layer, thus raising the velocity value of the bulk transport in the core of the channel. This also helps to increase the shear rates near the bottom wall and at the two fluids interface, increasing the drag force of the non-conducting fluid by the hydrodynamic viscous forces at the interface. Consequently, there is an increase in the dimensionless volumetric flow rate (cf. Fig. 6b). Fig. 6a also shows that in the absence of pressure gradient (and $R_\zeta = 0$) the EDL acts like a plate in pure Couette flow, generating a nearly constant shear stress across the channel.

Fig. 7 shows the dimensionless velocity profiles (a) and volumetric flow rate (b) at $\sqrt{\varepsilon}De_\kappa = 2$ (for comparison, the Newtonian results of Fig. 2 are also presented) to illustrate the effect of Γ . A favorable pressure gradient ($\Gamma < 0$) leads to an increase of the flow rate and makes velocity profiles fuller. By using also pressure forcing, which affects directly the two fluids, the flow rate quickly increases. The beneficial shear-thinning effect is clear in the large increase in the flow rate of Fig. 7b as compared to Fig. 2b, but the impact is stronger with the fluid B, where the shear-thinning is stronger, whereas the large viscosities in Fluid A limit the flow rate enhancement. As for the Newtonian-Newtonian fluid flow configuration, decreasing β leads to an increase in velocity profiles and the volumetric flow rate, which is further increased by shear-thinning effects (cf. Fig. 8a and b and compare with Fig. 3). When using a viscoelastic fluid as conducting fluid, it is natural to have a more viscous fluid than the Newtonian non-conducting fluid, which leads to an optimal flow situation.

The effects of the Fluid A holdup (R_A) and of the ratio of zeta potentials (R_ζ) are similar to what was described before, but now the viscoelastic flow exhibits a shear-thinning viscosity and the velocities have increased significantly near the bottom wall (see the higher values of u/u_{sh}) leading to the higher volumetric flow rates of Figs. 9 and 10, than in the corresponding constant viscosity case.

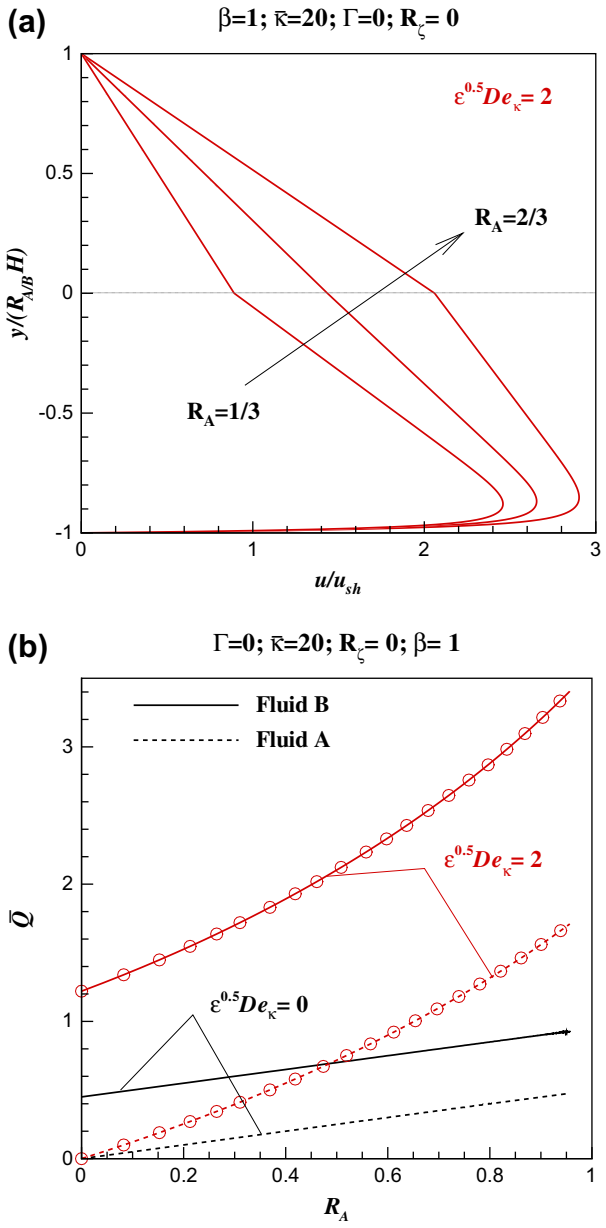

Fig. 10. Effect of the non-conducting fluid holdup on dimensionless (a) velocity profiles ($R_A = 1/3$, 1/2 and 2/3) and (b) volumetric flow rate for the Newtonian–viscoelastic flow configuration.

5. Conclusions

An analytical solution of the steady two-fluid electro-osmotic stratified flow in a planar microchannel is presented assuming a planar interface between the two viscoelastic immiscible fluids. The PTT fluid model was used, and the effects of fluid rheology, viscosity ratio, fluid holdup, and interfacial zeta potential were analyzed to show the viability of this pumping technique.

The flow can be induced by a combination of both electrical and pressure potentials, but in addition to the single contributions from these two mechanisms, when the conducting fluid is viscoelastic, there is an extra term in the velocity profile that simultaneously combines both effects, which is absent from conducting Newtonian fluids, in which the linear superposition principle applies. This work demonstrated that higher volumetric flow rates of a non-conducting Newtonian fluid can be achieved in EOF pumping when the conducting fluid is viscoelastic rather than Newtonian, due to the increase of the shear-thinning effects.

Acknowledgments

The authors would like to acknowledge financial support from FEDER and Fundação para a Ciência e a Tecnologia (FCT) through Project PTDC/EQU-FTT/113811/2009 and Scholarship SFRH/BPD/75436/2010 (A.M. Afonso).

References

[1] A. Brask, G. Goranovic, H. Bruus, Tech. Proc. Nanotech. 1 (2003) 190–193.
[2] Y. Gao, T.N. Wong, C. Yang, K.T. Ooi, J. Colloid Interf. Sci. 284 (1) (2005) 306–314.
[3] C.H. Chen, J.G. Santiago, J. Microelectromech. Syst. 11 (6) (2002) 672–683.
[4] X. Xuan, D. Li, J. Micromech. Microeng. 14 (2004) 290.
[5] X. Wang, C. Cheng, S. Wang, S. Liu, Microfluidics Nanofluidics 6 (2) (2009) 145–162.
[6] D. Laser, J. Santiago, J. Micromech. Microeng. 14 (2004) 290–298.
[7] S. Zeng, C.H. Chen, J.C. Mikkelsen, J.G. Santiago, Sens. Actuat. B: Chem. 79 (2–3) (2001) 107–114.
[8] S. Das, S. Chakraborty, Anal. Chim. Acta 559 (2006) 15–24.
[9] S. Chakraborty, Anal. Chim. Acta 605 (2007) 175–184.
[10] C.L.A. Berli, M.L. Olivares, J. Colloid Interf. Sci. 320 (2008) 582–589.
[11] A.M. Afonso, M.A. Alves, F.T. Pinho, J. Non-Newtonian Fluid Mech. 159 (2009) 50–63.
[12] N. Phan-Thien, R.I. Tanner, J. Non-Newtonian Fluid Mech. 2 (4) (1977) 353–365.
[13] N. Phan-Thien, J. Rheol. 22 (1978) 259–283.
[14] R.B. Bird, P.J. Dotson, N.L. Johnson, J. Non-Newtonian Fluid Mech 7 (1980) 213–235.
[15] H.M. Park, W.M. Lee, Lab on a Chip 8 (7) (2008) 1163–1170.
[16] A.M. Afonso, M.A. Alves, F.T. Pinho, J. Eng. Math. 71 (2011) 15–30.
[17] J.J. Sousa, A.M. Afonso, F.T. Pinho, M.A. Alves, Microfluidics Nanofluidics 10 (2011) 107–122.
[18] S. Dhinakaran, A.M. Afonso, M.A. Alves, F.T. Pinho, J. Colloid Interf. Sci. 344 (2010) 513–520.
[19] A.M. Afonso, F.T. Pinho, M.A. Alves, J. Non-Newtonian Fluid Mech. 179–180 (2012) 55–68.
[20] C. Yang, D. Li, J. Colloid Interf. Sci. 194 (1) (1997) 95–107.
[21] R.F. Probstein, Physicochemical Hydrodynamics: An Introduction, second ed., Hoboken, New Jersey, Wiley Interscience, New Jersey, USA, 2003.
[22] F.T. Pinho, P.J. Oliveira, J. Non-Newtonian Fluid Mech. 93 (2–3) (2000) 325–337.
[23] M.A. Alves, F.T. Pinho, P.J. Oliveira, J. Non-Newtonian Fluid Mech. 101 (2001) 55–76.